Spectral Analysis for Resonant Soft X-Ray Scattering Enables Measurement of Interfacial Width in 3D Organic Nanostructures

Thomas Ferron, Michael Pope, and Brian A. Collins

Phys. Rev. Lett. **119**, 167801 — Published 19 October 2017

DOI: 10.1103/PhysRevLett.119.167801

A spectral analysis for resonant soft X-ray scattering enables measurement of interfacial width in 3D organic nanostructures

Thomas Ferron, Michael Pope, and Brian A. Collins*

Department of Physics and Astronomy, Washington State University, Pullman, Washington 99164

Abstract: Interfaces are of critical importance to many materials and phenomena yet are difficult to probe. This difficulty is compounded in three-dimensional (3D) nanostructures and with delicate organic materials. Here we demonstrate a quantitative spectral analysis of resonant soft X-ray scattering that can accurately measure properties of buried nonplanar interfaces within polymeric systems. We measure the scattering invariant on an absolute scale to quantify the interfacial volume and width involved in mixing at the interface of block copolymer nanostructures. Using continuous contrast tuning, this spectral analysis enables the separation and identification of any number of unique scatterers in complex nanostructures.

Emergent phenomena and properties within materials and devices often originate at interfaces.[1–4] Thus, tools to study interfacial structure are of high importance but are rare, especially for organic or biological nanostructured devices or tissues that contain delicate, low-contrast, and nonplanar interfaces. Block copolymers (BCP) represent a good example of such materials. BCPs are molecules that consist of unique polymer segments connected through covalent bonds at the chain end and can thermodynamically phase separate into ordered 3D bulk nanostructures.[5] They are of particular interest for sub-10 nm photolithography[6,7] or bottom-up assembly of functional nanomaterials and devices.[8–10] Applications require a detailed understanding of the interfaces because sharpness and ordering of these interfaces will determine the limiting size of nanostructures[6] as well as optical or electronic coupling and interfacial states between the blocks.[10,11] Thus, interfacial width is a valuable parameter in optimizing BCP nanostructures.

Historically, methods employed to measure the nanometer-scale lateral structure and interfacial width include small angle scattering (SAS, via X-rays or neutrons, for example), dynamic secondary ion mass spectrometry (SIMS), and specular reflectivity. SAS experiments have attempted to utilize Porod's law at high scattering angles. However, limitations from low contrast and error-prone background subtractions make a determination of the interfacial width challenging.[12] SIMS measurements, on the other hand, are limited by low spatial resolution.[13] Instead, neutron specular reflectivity of polymer layers has been more successful, where a component is isotopically labelled in order to increase contrast. However, isotopic labeling can lead to alteration of interfacial parameters.[14] Specular reflectivity measurements are, furthermore, incapable of measuring lateral structures key in burgeoning technologies based on BCP materials.

Recent utilization of resonant soft X-rays at elemental absorption edges have begun to alleviate some difficulties presented in standard X-ray or neutron techniques.[15–17] Near an elemental absorption edge, a molecule's complex index of refraction $n(E) = 1 - \delta(E) + i\beta(E)$ fluctuates as a function of energy due to resonances involving electronic transitions from core atomic states to unoccupied molecular orbitals. Varying the photon energy effectively tunes molecular contrast, similar to isotopic labeling in neutron experiments, except resonant contrast is intrinsic to the molecule and tunable on a single sample.

To date, resonant soft X-ray scattering (RSoXS) has primarily been used in soft matter characterization to enhance scattering signal.[16,18–20] Quantitative spectral analyses and contrast tuning [21,22] have lagged inorganic systems[23–25] due to the complex nature of the molecular absorption fine structure. RSoXS allows for the chemical determination of scattering sources through spectral modeling because this fine structure encodes the chemical fingerprint of each molecule.[22] Sensitivity to transition dipole moments additionally enables correlative local measurements of molecular orientation.[26–28] To quantify these measurements, including BCP interfacial width, absolute scattering intensity is required. Unfortunately, while absolute SAS calibration standards have become increasingly available,[29] the low penetration depth of soft X-rays renders these resources unusable at absorption edges. Thus, independent experimental methods must be developed before quantitative measurements of these critical BCP interface phenomena can be realized.

In this letter we demonstrate both a quantitative spectral model for scattering across an absorption edge and a facile method to measure absolute scattering intensity that takes advantage of the historically undesirable X-ray fluorescence (XRF) background signal. This method enables measurement of potentially unlimited numbers of chemically independent molecular species in a composite nanostructure thin film. Through quantitative analysis of the scattering invariant, we extract both material phase and interface information of assembled 3D nanostructures of a model BCP, thus enabling high-precision measurements of nanostructure in soft matter.

The scattering invariant Q is defined as the overall scattering power of the sample and only depends on the mean square fluctuations of Δn. The invariant is so named because it does not depend on how those fluctuations are distributed in space (i.e. size of the structure); however, it does assume sharp interfaces between scatterers.[30] Mixing at these interfaces reduces the mean square fluctuation, and therefore, Q is sensitive to interfacial mixing if measured on an absolute scale. The scattering power is experimentally determined through an integral of scattering intensities $I(\boldsymbol{q}, E)$ over three dimensional reciprocal space $\boldsymbol{q}$ (the momentum transfer wave-vector, E is the photon energy). Since experimental measurements are constrained to a finite region in $\boldsymbol{q}$, we refer to these measurements as the total scattering intensity (TSI). In contrast, Q can be calculated by modeling an arbitrary number of domains contributing to scattering in a multidomain model adopted from Tatchev.[31] If we assume p domains separated by a discrete boundary

$$Q(E) = \frac{4\pi^2 V E^4}{(hc)^4} \sum_{i,j=1}^{p-1} \Delta n_{ip}(E) \Delta n_{jp}^*(E) \tilde{Q}_{ij} \tag{1}$$

where h is Planck's constant, c is the speed of light , V is the illuminated volume, Δn_{ij} is the difference in index of refraction between domains i and j, and $\tilde{Q}_{ij}$ is the partial invariant between those domains, which originates from the autocorrelation function or pair correlation function for diagonal terms and off diagonal terms, respectively. Equation (1) can be reduced to traditional two-phase expressions[30] by setting $p = 2$, and identifying $\tilde{Q}_{ij}$ as the product of volume fractions between domains i and j. This model enables one to separately incorporate scattering from multiple components. If the optical constants (index) are known for each component, then the scattering from each can be separately isolated, simplifying analysis.

In order to demonstrate the above model we investigated BCP poly(styrene-block-methyl methacrylate) (PS-b-PMMA) thin films of varying molecular weights, targeting specific internal nanostructures based on the molar ratio between components (lamellar, hexagonal close packed cylinders, and base-center cubic spheres – see Supporting Material for details of samples and their preparation).[5] Additionally, both blocks being coil-like, there is negligible X-ray dichroism or birefringence, allowing us to use scalar optical constants. This is important since molecular orientational correlations within nanostructures can occur with rod-like molecules, resulting in anisotropic scattering patterns that could complicate analysis.[26]

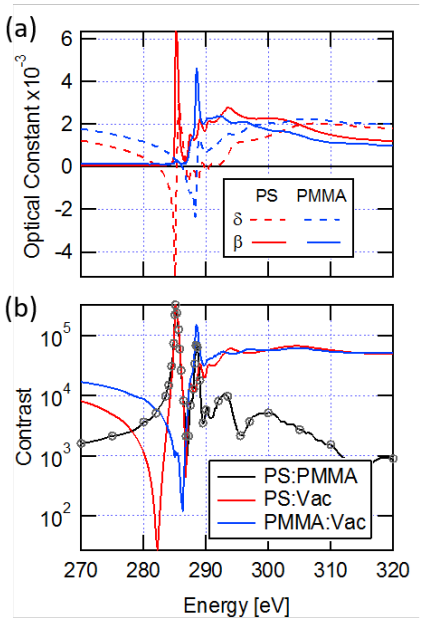

Figure 1: (a) Complex optical constants for PS and PMMA (b) Contrast functions $C = E^4 \Delta n_{AB}^2$ for three modeled domains: PS, PMMA, and Vacuum (arising from surface roughness). Circles indicate photon energies where RSoXS was measured.

Component optical constants shown in Figure 1a were calculated by Yan et al. via near edge X-ray absorption fine structure spectroscopy measurements on pure films of the polymer components.[32] Isolating unique molecular species experimentally is facile for synthetic molecules, and incorporating additional chemistry and orientation through calculations is improving dramatically.[33,34] In this study, three domains were taken into consideration: PS, PMMA, and vacuum. Vacuum is included here to incorporate scattering from surface roughness that is often the source of background that interferes with quantifying scattering signals. Therefore the three contrast functions in Figure 1b represent the possible sources of scattering signal. Each function exhibits a unique, rapidly changing

signal as a function of energy. Over the carbon edge, scattering contrast from these pairs varies by four orders of magnitude. Such a dramatic fluctuation arises from the fine structure in the optical constants and makes this technique particularly sensitive to multiple types of scatterers – allowing massive contrast enhancement at one energy and perfect contrast nulling at another. This variation is superior to deuteration for neutron scattering and eliminates the necessity of multiple, chemically altered samples.

Resonant Scattering in transmission geometry was completed at beamline 11.0.1.2 at the Advanced Light Source with detailed procedures previously reported.[35] Scattered energies utilized are indicated in Figure 1b. Lacking a soft X-ray calibration standard, we determine absolute scattering calibration through measurement of the 277 eV XRF background. Without energy discrimination in our detector, the measured signal I_m integrates both scattering and isotropic XRF

$$I_m(\boldsymbol{q},E) = R_r[I_{Scat}(\boldsymbol{q},E)\cdot T(E) + I_{XRF}(E)] \quad (2)$$

where and R_r is the relative responsivity between the GaAs photodiode and Princeton Instruments MTE CCD detector used to measure the incident and outgoing photon intensity, respectively. Transmittance through the sample $T(E)$ is measured directly at the location of scattering by the photodiode with and without the sample. Fluorescence intensity is calculated by the tabulated quantum yield of the carbon K_α transition ($\omega_{C_{K\alpha}} = 0.002575$)[36] and the number of absorbed photons (Figure S2) $I_{XRF}(E) = \omega_{C_{K\alpha}}[1 - T(E)]/4\pi$. The measured I_{XRF} is extracted as a constant background from I_m by fitting film scattering at high-q to a power law simultaneously at two separate energies – one above and one below the absorption edge (Figure S3). Comparing the measured and calculated XRF reveals the relative responsivity R_r between the detectors, enabling calibration of absolute scattering intensity to within 8% uncertainty, currently limited by beam stability.

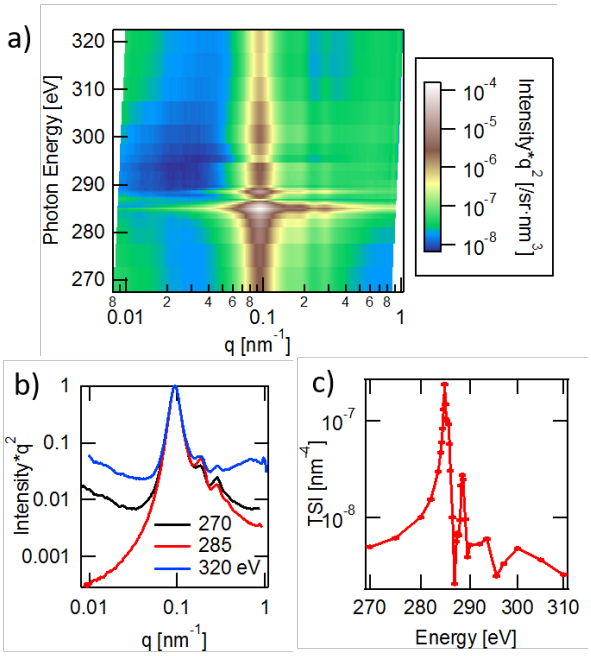

Figure 2: (a) Scattering intensity (*q^2 to accentuate features) as a function of both $|\mathbf{q}|$ and E. (b) Individual scattering profiles at select energies normalized to the BCP q^* peak. (c) Total scattering intensity as a function of energy.

RSoXS data for one sample across the carbon absorption edge are shown in Figure 2, which reveals significant structure as a function of both q and E. Select lineouts are shown in Figure 2b normalized to the primary BCP scattering peak at $q^* = 0.094\ nm^{-1}$, corresponding to a long period $L = 66.8\ nm$. Secondary peaks at $2q^*$ and $3q^*$ indicate the presence of lamellar nanostructure as predicted by the phase diagram for this sample. Interestingly, these profiles deviate from each other outside the primary peak, at both low and high-q. Profiles measured at a photon energy corresponding to the $\pi^*_{C=C}$ transition for PS (285.1eV) are qualitatively the most consistent with ideal BCP scattering as this is where the contrast function between PS and PMMA is maximized. In contrast, scattering from roughness dominates low-q regions and at energies both below and above the edge (Figure 2a). Fluorescence additionally dominates the high-q data above the edge (Figure 2a). $TSI(E)$ is given in Figure 2c and exhibits a rapidly changing signal. In fact, $TSI(E)$ near 286 eV fluctuates by more than two orders of magnitude over $\pm 1\ eV$, consistent with the contrast functions in Figure 1b.

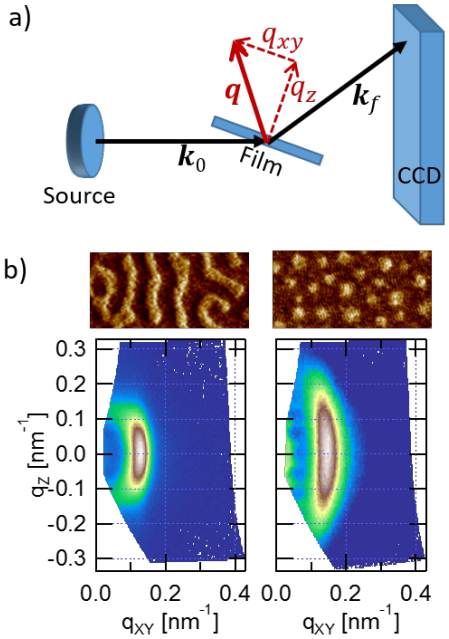

Figure 3: (a) Transmission scattering geometry enabling measurement of reciprocal space maps with one CCD exposure. k_0, k_f are the incident and scattered wavevectors, respectively. (b) Atomic force microscopy phase images and corresponding reciprocal space maps ($E = 285.1\ eV$) of a lamellar (left) and hexagonal close packed cylinder (right) BCP nanostructure.

Experimental measurement of the invariant has historically been accomplished by assuming isotropic scattering and is commonly used to measure the domain purity in polymer blend thin films.[19,37,38] As a consequence, vertical structure is ignored by considering only in-plane scattering in the traditional transmission geometry. In many cases thin films whose thickness is on the size scale of morphological features will have significantly different structure vertically versus in the film plane, resulting in cylindrical rather than spherical scattering symmetry. The required information could be obtained through a grazing incidence measurement. However, complex scattering models beyond the Born Approximation[39,40] are required to quantitatively interpret such data. Instead we retain the simplicity of transmission geometry by rotating the film from normal incidence to

20° as shown in Figure 3a. Rotating the sample will express the scattering component (q_z) perpendicular to the substrate and is shown for two samples in Figure 3b along with atomic force microscopy (AFM) of their lateral morphology. The scattering data demonstrate the elliptical patterns, which vary qualitatively by sample and thus must be measured directly. We correct our measured TSI through a ratio of the invariant calculated through cylindrical and spherical integration. Correction factors for all samples are given in Table S1 and often requires a $\pm 20\%$ correction, suggesting previous analyses of TSI for domain composition might contain errors on this level.[19,37,38]

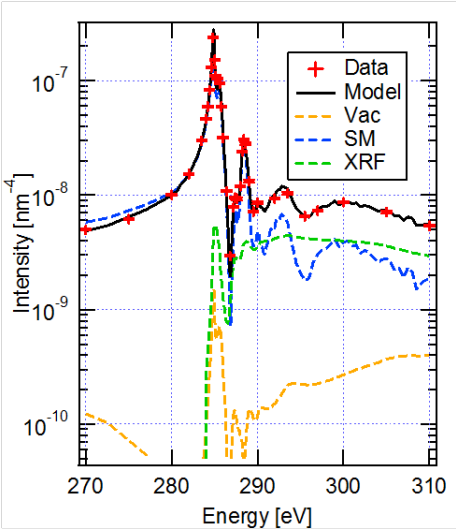

Figure 4: Example fit of the TSI data to the combined equations (1) and (2). Dashed are terms in the sum for the combined model defined in the text. Uncertainties are derived from detector statistics for scattering and optical constants.

By integrating equation (2) over $\boldsymbol{q}$, I_{scat} becomes Q and can be combined with equation (1). We fit the measured $TSI(E)$ to this combined model which contains only the four $\tilde{Q}_{ij}$ parameters plus an energy offset between the measured optical constants and the TSI data. The diagonal invariants represent material scattering between styrene and methacrylate domains $\tilde{Q}_{SM}$ and vacuum scattering from surface roughness $\tilde{Q}_{vac}$, while the off-diagonals represent cross correlations between the two. Simultaneous fitting over all samples is conducted to ensure an identical relative energy calibration. An example fit is illustrated in Figure 4 with all results shown in Figure S5. The only inputs to the model are the optical constants displayed in Figure 1 and the measured $T(E)$. Figure 4 also displays each source contribution resulting in the full model. Material scattering is responsible for approximately 90% of the total signal at lower energies. Above 290 eV, XRF and vacuum scattering (surface roughness) begin to contribute ~50% the signal making separate quantification important in analysis.

Interestingly, $\tilde{Q}_{Vac} \cong 0.01\tilde{Q}_{SM}$. This agrees with the relative volume of the surface region compared with the bulk where AFM measures an RMS roughness averaging about 1% of the total thickness. Using this relationship and tabulated atomic scattering factors[41] we calculate the expected scattering from surface roughness to make up 60% the total signal using hard X-rays at 10keV. Without precise methods to disentangle these two sources of scattering, accurate absolute measurement of domain scattering becomes impossible.

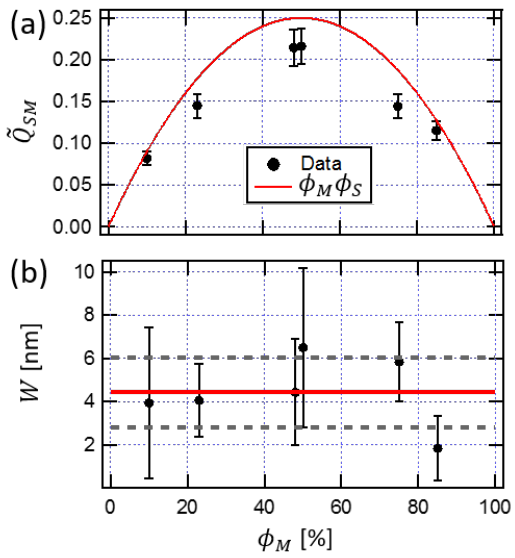

Figure 5: (a) Partial invariant corresponding to domain scattering plotted against sample PMMA volume fraction ϕ_M. Data (black circles) compared to calculation (line) assuming sharp interfaces. (b) Calculated interfacial width modeled as an error function. Average value (line) and standard deviation (dash) are shown. Uncertainties propagated from fit results and absolute scattering calibration.

$\tilde{Q}_{SM}$ equals the product of volume fractions for the two components assuming sharp interfaces and is plotted as the red line in Figure 5a as a function of the known volume fraction of PMMA (ϕ_M). Qualitatively, the extracted values follow the expected trend. However, the measurements are systematically lower than predicted. This is because entropic mixing of the two polymer components at the BCP interfaces reduces the mean squared fluctuation within the sample and therefore the measured scattering. This reduction originates from an effective volume or *interphase* region that does not contribute to the scattering. The composition across the interface can be modeled as an error function and the effective interphase can be subtracted from the scattering volume using $\tilde{Q}_{SM} = \phi_S\phi_M - \frac{\sqrt{2}}{2\pi}\frac{S}{V}W$,[30] where S is the total area of the interface, V is the sample volume, and W is the interfacial width. If we assume a perfectly constructed lattice following the BCP phase diagram, we can calculate S/V for each morphology leaving only W as an unknown parameter. Figure 5b gives the resulting interfacial width measurement with an average of $W = 4.4 \pm 0.7\ nm$. This is slightly lower than the width for these materials measured with reflectivity ($5.0\ nm$)[15] yet agrees within the uncertainty. The error bars are dominated by poor beam stability reported previously.[28] Significantly higher accuracy could be achieved with improvements of the beamline and in beamlines currently under construction.

This measurement is remarkable, first because the spectral model we use isolates domain scattering cleanly from other sources such as roughness scattering, absorption, and fluorescence effects. As there are no constraints on p in Equation (1), this method could easily be expanded to systems containing an arbitrary number of unique molecular species in ordered structures and is free of the need for laborious and potentially disruptive labelling techniques. Without the intrinsic contrast variation at the absorption edge, this measurement is nearly impossible. In this application, we furthermore demonstrate quantitative measurement of a nonplanar interface which is impossible with specular reflectivity – the only other successful direct measurement of interfacial width. In fact,

reflectivity convolutes interfacial width with capillary fluctuations of the position of the interface. Our method removes this limitation and the narrower width we measure may actually be closer to the intrinsic interfacial width for this system. Although our polymers are well classified in the strong segregation limit,[6] with improved precision this method could additionally contribute to thermodynamic investigation below this limit. Conversely, if W is known, the specific area S/V of the interface is accessible as well. Putting these advantages together, our method is well suited for future investigations into sub-10nm patterning or functional nanostructures and devices.[6–10]

In conclusion, we have employed a novel absolute scattering calibration and multidomain spectral model for RSoXS to determine the interfacial width of three-dimensional polymer nanostructures. The model identifies and isolates the sources of resonant scattering over the carbon K_α absorption edge enabling high precision measurements. We show that over a range of BCP nanostructures the measured interfacial width agrees with previous measurements on planar structures. Our study allows for the direct measurement of interface properties in an assembled 3D nanostructure, and with appropriately quantified optical constants, this application can extend to any elemental absorption edge or molecular material.

Dean Delongchamp, Daniel Sunday, and Wen-Li Wu are gratefully acknowledged for their discussions regarding the intersection of polymer physics and scattering. T. Ferron acknowledges support from the Washington State University Seed Grant for this work. This research used resources of the Advanced Light Source, which is a DOE Office of Science User Facility under contract no. DE-AC02-05CH11231.

*To whom all correspondence should be addressed: brian.collins@wsu.edu

1. Soumyanarayanan, A., Reyren, N., Fert, A., and Panagopoulos, C. "**Emergent Phenomena Induced by Spin–orbit Coupling at Surfaces and Interfaces**" *Nature* 539, no. 7630 (2016): 509–517. doi:10.1038/nature19820, Available at http://www.nature.com/doifinder/10.1038/nature19820

2. Vandewal, K., Albrecht, S., Hoke, E. T., Graham, K. R., Widmer, J., Douglas, J. D., Schubert, M., Mateker, W. R., Bloking, J. T., Burkhard, G. F., Sellinger, A., Frechet, J. M. J., Amassian, A., Riede, M. K., McGehee, M. D., Neher, D., and Salleo, A. "**Efficient Charge Generation by Relaxed Charge-Transfer States at Organic Interfaces**" *Nat Mater* 13, no. 1 (2014): 63–68. doi:10.1038/nmat3807, Available at http://www.ncbi.nlm.nih.gov/pubmed/24240240

3. Jailaubekov, A. E., Willard, A. P., Tritsch, J. R., Chan, W.-L., Sai, N., Gearba, R., Kaake, L. G., Williams, K. J., Leung, K., Rossky, P. J., and Zhu, X.-Y. "**Hot Charge-Transfer Excitons Set the Time Limit for Charge Separation at Donor/acceptor Interfaces in Organic Photovoltaics.**" *Nature materials* 12, no. 1 (2013): 66–73. doi:10.1038/nmat3500, Available at http://dx.doi.org/10.1038/nmat3500

4. Birol, T., Benedek, N. A., and Fennie, C. J. "**Interface Control of Emergent Ferroic Order in Ruddlesden-Popper Sr N + 1 Ti N O 3 N + 1**" *Physical Review Letters* 107, no. 25 (2011): 257602. doi:10.1103/PhysRevLett.107.257602, Available at https://link.aps.org/doi/10.1103/PhysRevLett.107.257602

5. Bates, F. S. and Fredrickson, G. H. "**Block Copolymer Thermodynamics: Theory and Experiment**" *Annual Review of Physical Chemistry* 41, no. 1 (1990): 525–557. doi:10.1146/annurev.pc.41.100190.002521, Available at http://dx.doi.org/10.1146/annurev.pc.41.100190.002521

6. Sinturel, C., Bates, F. S., and Hillmyer, M. A. "**High χ–Low *N* Block Polymers: How Far Can We Go?**" *ACS Macro*

Letters 4, no. 9 (2015): 1044–1050. doi:10.1021/acsmacrolett.5b00472, Available at http://pubs.acs.org/doi/10.1021/acsmacrolett.5b00472

7. Chang, T.-H., Xiong, S., Jacobberger, R. M., Mikael, S., Suh, H. S., Liu, C.-C., Geng, D., Wang, X., Arnold, M. S., Ma, Z., and Nealey, P. F. "**Directed Self-Assembly of Block Copolymer Films on Atomically-Thin Graphene Chemical Patterns**" *Scientific Reports* 6, no. 1 (2016): 31407. doi:10.1038/srep31407, Available at http://www.nature.com/articles/srep31407

8. Thorkelsson, K., Bai, P., and Xu, T. "**Self-Assembly and Applications of Anisotropic Nanomaterials: A Review**" *Nano Today* 10, no. 1 (2015): 48–66. doi:10.1016/j.nantod.2014.12.005

9. Kao, J., Thorkelsson, K., Bai, P., Zhang, Z., Sun, C., and Xu, T. "**Rapid Fabrication of Hierarchically Structured Supramolecular Nanocomposite Thin Films in One Minute**" *Nature Communications* 5, (2014): 4053. doi:10.1038/ncomms5053, Available at http://www.ncbi.nlm.nih.gov/pubmed/24887144

10. Guo, C. H., Lin, Y. H., Witman, M. D., Smith, K. A., Wang, C., Hexemer, A., Strzalka, J., Gomez, E. D., and Verduzco, R. "**Conjugated Block Copolymer Photovoltaics with near 3% Efficiency through Microphase Separation**" *Nano Letters* 13, no. 6 (2013): 2957–2963. doi:Doi 10.1021/Nl401420s

11. Grieco, C., Aplan, M. P., Rimshaw, A., Lee, Y., Le, T. P., Zhang, W., Wang, Q., Milner, S. T., Gomez, E. D., and Asbury, J. B. "**Molecular Rectification in Conjugated Block Copolymer Photovoltaics**" *Journal of Physical Chemistry C* 120, no. 13 (2016): 6978–6988. doi:10.1021/acs.jpcc.6b00103

12. Perrin, P. and Prud'homme, R. E. "**SAXS Measurements of Interfacial Thickness in Amorphous Polymer Blends Containing a Diblock Copolymer**" *Macromolecules* 27, (1994): 1852–1860.

13. Reynolds, B. J., Ruegg, M. L., Mates, T. E., Radke, C. J., and Balsara, N. P. "**Experimental and Theoretical Study of The Adsorption of a Diblock Copolymer to Interfaces between Two Homopolymers**" *Macromolecules* 38, no. 9 (2005): 3872–3882. doi:10.1021/ma047539s

14. Xhb, X. and Russell, T. P. "**Changes in Polystyrene and Poly(methy1 Methacrylate) Interactions with Isotopic Substitution Table I. Flory-Huggins Interaction Parameter for PS and PMMA Diblock Copolymers**" *Macromolecules* 26, (1993):

15. Sunday, D. F. and Kline, R. J. "**Reducing Block Copolymer Interfacial Widths through Polymer Additives**" *Macromolecules* (2015): doi:10.1021/ma502015u

16. Virgili, J. M., Tao, Y. F., Kortright, J. B., Balsara, N. P., and Segalman, R. A. "**Analysis of Order Formation in Block Copolymer Thin Films Using Resonant Soft X-Ray Scattering**" *Macromolecules* 40, no. 6 (2007): 2092–2099. doi:10.1021/ma061734k

17. Wang, C., Garcia, A., Yan, H. P., Sohn, K. E., Hexemer, A., Nguyen, T. Q., Bazan, G. C., Kramer, E. J., and Ade, H. "**Interfacial Widths of Conjugated Polymer Bilayers**" *J Am Chem Soc* 131, no. 35 (2009): 12538. doi:Doi 10.1021/Ja905293m

18. Mitchell, G. E., Landes, B. G., Lyons, J., Kern, B. J., Devon, M. J., Koprinarov, I., Gullikson, E. M., and Kortright, J. B. "**Molecular Bond Selective X-Ray Scattering for Nanoscale Analysis of Soft Matter**" *Applied Physics Letters* 89, no. 4 (2006): 1–4. doi:10.1063/1.2234301

19. Collins, B. A., Li, Z., Tumbleston, J. R., Gann, E., McNeill, C. R., and Ade, H. "**Absolute Measurement of Domain Composition and Nanoscale Size Distribution Explains Performance in PTB7:PC71BM Solar Cells**" *Advanced Energy Materials* 3, no. 1 (2013): 65–74. doi:10.1002/aenm.201200377, Available at

http://onlinelibrary.wiley.com/doi/10.1002/aenm.201200377/abstract

20. Sunday, D. F., Hammond, M. R., Wang, C., Wu, W., Delongchamp, D. M., Tjio, M., Cheng, J. Y., Pitera, J. W., and Kline, R. J. "**Determination of the Internal Morphology of Nanostructures Patterned by Directed Self Assembly**" *Acs Nano* 8, no. 8 (2014): 8426–8437. doi:10.1021/nn5029289, Available at http://dx.doi.org/10.1021/nn5029289

21. Wang, C., Lee, D. H., Hexemer, A., Kim, M. I., Zhao, W., Hasegawa, H., Ade, H., and Russell, T. P. "**Defining the Nanostructured Morphology of Triblock Copolymers Using Resonant Soft X-Ray Scattering**" *Nano Letters* 11, no. 9 (2011): 3906–3911. doi:Doi 10.1021/Nl2020526

22. Wong, D. T., Wang, C., Beers, K. M., Kortright, J. B., and Balsara, N. P. "**Mesoporous Block Copolymer Morphology Studied by Contrast-Matched Resonant Soft X-Ray Scattering**" *Macromolecules* (2012): doi:10.1021/ma3019206, Available at http://pubs.acs.org/doi/abs/10.1021/ma3019206

23. Smadici, S., Lee, J. C. T., Wang, S., Abbamonte, P., Logvenov, G., Gozar, A., Cavellin, C. D., and Bozovic, I. "**Superconducting Transition at 38 K in Insulating-Overdoped La2CuO4-La1.64Sr0.36CuO4 Superlattices: Evidence for Interface Electronic Redistribution from Resonant Soft X-Ray Scattering**" *Physical Review Letters* 102, no. 10 (2009): 1–4. doi:10.1103/PhysRevLett.102.107004

24. Abbamonte, P., Rusydi, A., Smadici, S., Gu, G. D., Sawatzky, G. A., and Feng, D. L. "**Spatially Modulated 'Mottness' in La2-xBaxCuO4**" *Nature Physics* 1, no. 3 (2005): 155–158. doi:10.1038/nphys178, Available at http://dx.doi.org/10.1038/nphys178

25. Collins, B. A., Chu, Y. S., He, L., Haskel, D., and Tsui, F. "**Structural and Chemical Ordering of Heusler CoxMnyGez Epitaxial Films on Ge (111): Quantitative Study Using Traditional and Anomalous X-Ray Diffraction Techniques**" *Physical Review B* 92, no. 22 (2015): 224108. doi:10.1103/PhysRevB.92.224108, Available at http://link.aps.org/doi/10.1103/PhysRevB.92.224108

26. Collins, B. A., Cochran, J. E., Yan, H., Gann, E., Hub, C., Fink, R., Wang, C., Schuettfort, T., McNeill, C. R., Chabinyc, M. L., and Ade, H. "**Polarized X-Ray Scattering Reveals Non-Crystalline Orientational Ordering in Organic Films**" *Nature Materials* 11, no. 6 (2012): 536–543. doi:10.1038/nmat3310, Available at http://www.nature.com/nmat/journal/v11/n6/full/nmat3310.html

27. Tumbleston, J. R., Collins, B. A., Yang, L., Stuart, A. C., Gann, E., Ma, W., You, W., and Ade, H. "**The Influence of Molecular Orientation on Organic Bulk Heterojunction Solar Cells**" *Nature Photonics* (2014): doi:10.1038/nphoton.2014.55, Available at http://gateway.webofknowledge.com/gateway/Gateway.cgi?GWVersion=2&SrcAuth=ORCID&SrcApp=OrcidOrg&DestLinkType=FullRecord&DestApp=WOS_CPL&KeyUT=WOS:000335011700013&KeyUID=WOS:000335011700013

28. Stone, K. H. and Kortright, J. B. "**Molecular Anisotropy Effects in Carbon K -Edge Scattering: Depolarized Diffuse Scattering and Optical Anisotropy**" *Physical Review B* 90, no. 10 (2014): 104201. doi:10.1103/PhysRevB.90.104201

29. Allen, A. J., Zhang, F., Joseph Kline, R., Guthrie, W. F., and Ilavsky, J. "**NIST Standard Reference Material 3600: Absolute Intensity Calibration Standard for Small-Angle X-Ray Scattering**" *Journal of Applied Crystallography* (2017): doi:10.1107/S1600576717001972

30. Roe, R.-J. J. "**Methods of X-Ray and Neutron Scattering in Polymer Science**" (2000): Available at http://www.amazon.com/Methods-Neutron-Scattering-Polymer-Science/dp/0195113217

31. Tatchev, D. "**Multiphase Approximation for Small-Angle Scattering**" *Journal of Applied Crystallography* 43, no. 1 (2010): 8–11. doi:doi:10.1107/S0021889809048675, Available at http://dx.doi.org/10.1107/S0021889809048675

32. Yan, H., Wang, C., McCarn, A. R., and Ade, H. "**Accurate and Facile Determination of the Index of Refraction of Organic Thin Films Near the Carbon 1s Absorption Edge**" *Physical Review Letters* 110, no. 17 (2013): 177401. doi:10.1103/PhysRevLett.110.177401, Available at http://link.aps.org/doi/10.1103/PhysRevLett.110.177401

33. Urquhart, S. G., Martinson, M., Eger, S., Murcia, V., Ade, H., and Collins, B. A. "**Connecting Molecular Conformation to Aggregation in P3HT Using near Edge X-Ray Absorption Fine Structure Spectroscopy**" *Submitted* (2017):

34. Sunday, D. F., Chan, E. P., Orski, S. V., Nieuwendaal, R. C., and Stafford, C. M. "**Evaluating the Network Structure of Desalination Nanomembranes via Functional Group Quantification with Soft X-Ray Reflectivity**" *Submitted* (2017):

35. Gann, E., Young, A. T., Collins, B. A., Yan, H., Nasiatka, J., Padmore, H. A., Ade, H., Hexemer, A., and Wang, C. "**Soft X-Ray Scattering Facility at the Advanced Light Source with Real-Time Data Processing and Analysis**" *Review of Scientific Instruments* 83, no. 4 (2012): 45110. doi:10.1063/1.3701831, Available at http://gateway.webofknowledge.com/gateway/Gateway.cgi?GWVersion=2&SrcAuth=ORCID&SrcApp=OrcidOrg&DestLinkType=FullRecord&DestApp=WOS_CPL&KeyUT=WOS:000303415300072&KeyUID=WOS:000303415300072

36. Hubbell, J. H., Trehan, P. N., Singh, N., Chand, B., Mehta, D., Garg, M. L., Garg, R. R., Singh, S., and Puri, S. "**A Review, Bibliography, and Tabulation of K, L, and Higher Atomic Shell X□Ray Fluorescence Yields**" *Journal of Physical and Chemical Reference Data* 23, no. 2 (1994): 339–364. doi:10.1063/1.555955, Available at http://scitation.aip.org/content/aip/journal/jpcrd/23/2/10.1063/1.555955

37. Liu, Y. H., Zhao, J. B., Li, Z. K., Mu, C., Ma, W., Hu, H. W., Jiang, K., Lin, H. R., Ade, H., and Yan, H. "**Aggregation and Morphology Control Enables Multiple Cases of High-Efficiency Polymer Solar Cells**" *Nature Communications* 5, (2014): 1–8. doi:Artn 5293Doi 10.1038/Ncomms6293, Available at http://www.nature.com/ncomms/2014/141110/ncomms6293/pdf/ncomms6293.pdf

38. Carpenter, J. H., Hunt, A., and Ade, H. "**Characterizing Morphology in Organic Systems with Resonant Soft X-Ray Scattering**" *Journal of Electron Spectroscopy and Related Phenomena* 200, (2015): 2–14. doi:10.1016/j.elspec.2015.05.006, Available at http://dx.doi.org/10.1016/j.elspec.2015.05.006

39. Gann, E., Watson, A., Tumbleston, J. R., Cochran, J., Yan, H., Wang, C., Seok, J., Chabinyc, M., and Ade, H. "**Topographic Measurement of Buried Thin-Film Interfaces Using a Grazing Resonant Soft X-Ray Scattering Technique**" *Physical Review B* 90, no. 24 (2014): 245421. doi:10.1103/PhysRevB.90.245421

40. Hexemer, A. and Muller-Buschbaum, P. "**Advanced Grazing-Incidence Techniques for Modern Soft-Matter Materials Analysis**" *IUCrJ* 2, (2015): 106–125. doi:10.1107/S2052252514024178

41. Henke, B. L., Gullikson, E. M., and Davis, J. C. "**X-Ray Interactions: Photoabsorption, Scattering, Transmission, and Reflection at E = 50-30,000 eV, Z = 1-92**" *Atomic Data and Nuclear Data Tables* 54, no. 2 (1993): 181–342. doi:10.1006/adnd.1993.1013, Available at http://www.sciencedirect.com/science/article/B6WBB-45R7DJM-8/2/70158a249f3de7a951a3ae98a0b114ab